PHYSICAL REVIEW B VOLUME 24, NUMBER 12 15 DECEMBER 1981

Optical properties of single-crystal rutile RuO_2 and IrO_2 in the range 0.5 to 9.5 eV

Ashok K. Goel,* G. Skorinko, and Fred H. Pollak
Department of Physics, Brooklyn College of City University of New York, Brooklyn, New York 11210
(Received 21 May 1981)

We have measured the near-normal incidence reflectivity of single-crystal rutile RuO_2 and IrO_2 for $\vec{E}||c$ axis and $\vec{E}\perp c$ axis at room temperature in the photon energy range 0.5–9.5 eV. From a Kramers-Kronig analysis of the reflectivity we have obtained the spectral dependence of the real and imaginary parts of the complex dielectric constant (ϵ_1 and ϵ_2, respectively) and refractive index (n and k, respectively) for each material. Comparison with recent band-structure and density-of-states calculations and past experimental studies of related solids has enabled us to gain further insight into the nature of the oxygen p electrons and metal d electrons in these materials.

I. INTRODUCTION

Ruthenium dioxide, RuO_2, and iridium dioxide, IrO_2, belong to the family of transition-metal dioxide compounds with rutile-type structure which possess an interesting variety of electrical and magnetic properties. RuO_2 is well known as a corrosion-resistant low-overpotential electrode for chlorine evolution.[1,2] Because of its low-anodic-oxygen overpotential, RuO_2 has been shown to be an equally effective electrode for oxygen evolution.[3–5] Furthermore, it has recently been reported that the catalytic photodecomposition of water into hydrogen and oxygen proceeds at a much higher rate when RuO_2 is added to a TiO_2 electode.[6] These latter properties are particularly significant should hydrogen generation via water decomposition (either electrolysis or photoelectrolysis) become a part of any future energy program. In addition, because of its high electrical conductivity and chemical stabililty, RuO_2 shows great promise as an electrical contact material[7] and strip-line conductor in integrated circuits.[8]

The performance of an IrO_2 anode has also been found to be much superior to that of pure Pt for the oxygen evolution reaction.[9,10] Recently, the search for effective passive display devices has stimulated much interest in electrochromism,[11] a reversible color change induced electrochemically. An anodically grown iridium oxide film has been reported[12,13] to be a very promising electrochromic material and this has prompted several recent studies of their properties.[14–20] Its advantages over other electrochromic oxides such as WO_3 are shown to include (i) fast response, (ii) good open-circuit memory, (iii) ability not to degrade in the presence of water, and (iv) the ability to grow and reform the oxide layer *in situ* in the electro-optic display cell.[12] As regards single crystals, the electrical-transport properties of RuO_2 and IrO_2 have been reported by Ryden *et al.*[21] and the conduction-electron screening effects have been demonstrated in IrO_2 by Wertheim and Guggenheim.[22] The above interesting properties of RuO_2 and IrO_2 are related to the nature of the metal d electrons. Although a considerable amount of applied research[23] has been performed on the properties of RuO_2 and IrO_2, little work has been done on their fundamental aspects.

In this paper, we present the first comprehensive optical investigation of single-crystal RuO_2 and IrO_2. We have measured the near-normal incidence ($\sim 6°$) reflectivity for the electric-field vector $\vec{E}$ of the light polarized parallel ($||$) and perpendicular ($\perp$) to the c axis in the energy range 0.5 to 9.5 eV at room temperature. Real and imaginary parts of the complex dielectric constant and refractive index have then been deduced for each crystal from a Kramers-Kronig analysis of the reflectivity. These quantites have been compared with some recent band-structure and density-of-states calculations as well as past experimental studies of related solids TiO_2 (Ref. 24) and VO_2 (Ref. 25) in order to gain further insight into the nature of the oxygen p electrons and metal d electrons in these materials.

II. EXPERIMENTAL DETAILS

Single crystals of RuO_2 were grown in our laboratory by the method of chemical transport reac-

tion in a flowing system. This technique is similar to that used by Reames[26] and more recently by Shafer *et al.*[27] In the presence of oxygen at 800–1500 °C gaseous oxides (RuO_3 and IrO_3) exist. The reaction takes place by the mechanism

$$M(\text{solid})+\tfrac{3}{2}O_2 \rightarrow MO_3(\text{gas}) ,$$

where $M=$Ru or Ir. The volatile MO_3 gas dissociates to MO_2 in the cooler region. In our procedure, several grams of the Ru powder were contained in an alumina source boat. This boat was placed inside a Mullite tube at the center of the furnace which was raised to a temperature of 1400 °C. Oxygen at atmospheric pressure was passed through the Mullite tube at a flow rate of about 15 cm^3/min. A second boat, which acted as a substrate, was placed 210 cm from the source boat in a cooler portion of the furnace (about 1000 °C). After several days, crystals of dimensions up to $6\times4\times2$ mm^3 had formed in the substrate boat. Single crystals of IrO_2 were supplied by F. M. Reames.

A number of crystals were examined by x-ray diffraction and Laue backscattering which indicated that they were of relatively good quality. Crystal faces were oriented perpendicular to the a axis by the x-ray diffraction method to $\pm1°$. They were then polished by using 12-μm alumina powder, 6-μm diamond paste, 3- and 0.3-μm alumina powders and finally polish etched using Siton.[28]

A high-precision rotating-light pipe reflectometer[29] was used in order to record the reflectivity R as a continous function of wavelength. The entire wavelength range was divided into three parts: near infrared (20 000 to 7000 Å), visible (7000 to 2800 Å) and ultraviolet (2800 to 1200 Å). Light sources were a 150-W xenon lamp and tungsten-halogen lamp in the visible and infrared ranges, respectively. A McPherson Model 630 H_2-gas-discharge lamp was used as the light source in the ultraviolet part. Polarization of the incident radiation was achieved by using appropriate Polaroid sheet polarizers in the visible and infrared. In the ultraviolet region, polarization was accomplished by reflection from a cleaved LiF plate at the Brewster angle. A photomultiplier was used as the detector in the visible range and PbS cell was employed in the infrared region. A prism predisperser was installed in front of the entrance slit of the mononchromator in the visible part to avoid second-order effects and to minimize the scattered light, while in the infrared range the radiation below 7000 Å was filtered out with the help of a high-pass filter. In the ultraviolet, measurements were carried out in vacuum ($\sim10^{-6}$ Torr). Mirrors coated with MgF_2 were used in this range which highly enhances the reflectivity of uv radiation down to 1200 Å. In this region, the front surface of the light pipe was coated with a thin and uniform film of sodium salicylate which converts ultraviolet radiation into visible light so that a photomultiplier could be used. Further experimental details are described in Refs. 30 and 31.

In the case of an isotropic crystal, when the angle of incidence of the incident radiation is not normal to the surface of the solid, then the reflected intensity is given by

$$R_n=\frac{(a-\cos\phi)^2+b^2}{(a+\cos\phi)^2+b^2} \tag{1}$$

and

$$R_p=R_n\frac{(a-\sin\phi\tan\phi)^2+b^2}{(a+\sin\phi\tan\phi)^2+b^2} \tag{2}$$

where $R_n(R_p)$ is reflected intensity of the solid when the polarization of the incident radiation is perpendicular (parallel) to the plane of incidence and ϕ is the angle between the incident radiation and the normal to the surface of the solid. The parameters a^2 and b^2 are related to φ and the optical constants n and k by the relations

$$a^2=\tfrac{1}{2}\{[(n^2-k^2-\sin^2\phi)^2+4n^2k^2]^{1/2}+(n^2-k^2-\sin^2\phi)\} ,$$

$$b^2=\tfrac{1}{2}\{[(n^2-k^2-\sin^2\phi)^2+4n^2k^2]^{1/2}-(n^2-k^2-\sin^2\phi)\} .$$

RuO_2 and IrO_2 are anistropic crystals of the uniaxial type, i.e., they have dielectric constants of the form $\epsilon_x=\epsilon_y\neq\epsilon_z$. For these crystals, R_n as given by Eq. (1) can still be used if any one of the principal axes of the crystal is taken in the direction perpendicular to the plane of incidence and R_p in Eq. (2) can still be used if the c axis is in the direction perpendicular to the plane of incidence, as was the case in our experiments. Experimentally, R_n and R_p were measured at several values of ϕ (from 5° to 75° in steps of 5°, depending upon the size of the crystal) for the laser energies 1.96, 2.53, and 2.73 eV. The values of a and b (and hence n and k) were then obtained by a χ^2 fit between the theoretically expected and experimentally found reflectivity values. The values of ϵ_1 and ϵ_2 were then deter-

mined for each of the laser energies from the relations $\epsilon_1 = n^2 - k^2$ and $\epsilon_2 = 2nk$.

III. EXPERIMENTAL RESULTS

The polarization dependent near-normal incidence reflectivity at room temperature of single crystal RuO_2 in the range 0.5—9.5 eV is shown in Fig. 1. The spectra for both $\vec{E}||c$ and $\vec{E}\perp c$ have four major features that are denoted by A, B_1, C_1, and E. In addition, there are smaller structures indicated by B_2, B_3, C_2, and D. At ~ 1 eV the feature A has a well-resolved peak for $\vec{E}||c$ and a shoulder for $\vec{E}\perp c$. Although the reflectivity curves for the two polarization directions are quite similar there are differences in energy positions for some of the features. For example, $B_1^{\parallel}$ and $E^{\parallel}$ occur at ~ 0.15 eV below $B_1^{\perp}$ and $E^{\perp}$, respectively. The feature B_2 is present for both the polarizations at nearly the same energy but the shoulder $C_2^{\parallel}$ does not have its counterpart for $\vec{E}\perp c$; the same is true for $B_3^{\perp}$ which does not appear for $\vec{E}||c$.

Figure 2 shows the near-normal incidence room-temperature reflectivity spectra of single crystal IrO_2 for both $\vec{E}||c$ and $\vec{E}\perp c$ in the photon energy range 0.5—9.5 eV. Curves for both the polarizations have four major features which are denoted by A, B_1, C_1, and E. In addition, there are smaller structures indicated by A_2, A_3, B_2, C_2, and D. Although the reflectivity spectra for both $\vec{E}||c$ and $\vec{E}\perp c$ are quite similar there are significant differences in energy positions for most of the features. Almost all the features for $\vec{E}||c$ appear at higher energies than their counterparts for $\vec{E}\perp c$. For example, $A_2^{\parallel}$ is observed ~ 0.2 eV above $A_2^{\perp}$, $B_1^{\parallel}$ occurs at ~ 0.4 eV above $B_1^{\perp}$, $C_1^{\parallel}$ appears at ~ 0.7 eV above $C_1^{\perp}$ and $E^{\parallel}$ is present ~ 0.2 eV above $E^{\perp}$. Small structure $D^{\parallel}$ is observed ~ 1 eV above $D^{\perp}$. Some features appear for one of the polarizations only. For example, C_2 appears only for $\vec{E}||c$ having no counterpart for $\vec{E}\perp c$, while B_2 is observed for $\vec{E}\perp c$ only. Dotted lines represent extrapolations of the reflectivity down to 0 eV.

Quantities more relevant for the discussion of the electronic states of the solid are the optical constants rather than the reflectivity spectra. We have deduced the real (ϵ_1) and imaginary (ϵ_2) parts of the complex dielectric constant as well as real (n) and imaginary (k) parts of the complex refractive index by means of a Kramers-Kronig (KK) analysis of the reflectivity. An extrapolation scheme was used to evaluate the (KK) integral. In this method, the reflectivity R at an energy above the upper limit of the measurement (~ 9.5 eV) was taken to be $R = R_1(\hbar\omega_1/\hbar\omega)^{\beta}$, where $\hbar\omega_1$ is the upper limit of the measurements, R_1 is the reflectivity at $\hbar\omega_1$, and β is an adjustable parameter.[31,32] The parameter β was fit by requiring the optical constants to agree with values determined by angular reflectivity measurements at the laser energies 1.96, 2.53, and 2.73 eV.[30,31]

Room-temperature spectra of ϵ_1 and ϵ_2 for RuO_2 are given in Figs. 3 and 4, respectively, both for $\vec{E}||c$ and $\vec{E}\perp c$ in the energy range 0.5—9.5 eV. Spectra of n and k for RuO_2 are shown in Figs. 5 and 6, respectively. For IrO_2, ϵ_1 and ϵ_2 spectra for $\vec{E}||c$ and $\vec{E}\perp c$ in the energy range 0.5—9.5 eV are plotted in Figs. 7 and 8, respectively. Figures 9 and 10 show the n and k spectra, respectively, for

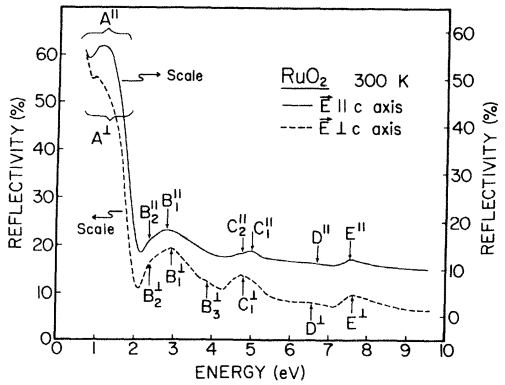

FIG. 1. Near-normal incidence reflectivity of single-crystal rutile RuO_2 at room temperature for $\vec{E}||c$ and $\vec{E}\perp c$ in the energy range 0.5—9.5 eV.

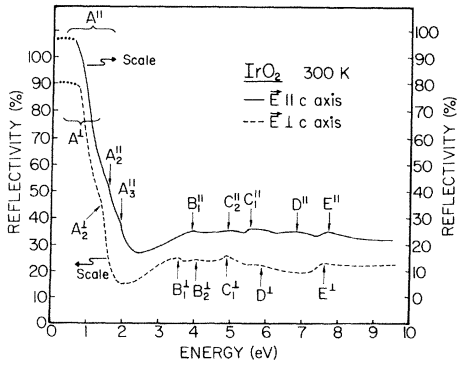

FIG. 2. Near-normal incidence reflectivity of single-crystal rutile IrO_2 at room temperature for $\vec{E}||c$ and $\vec{E}\perp c$ in the energy range 0.5—9.5 eV. Dotted lines represent the extrapolation of the reflectivity.

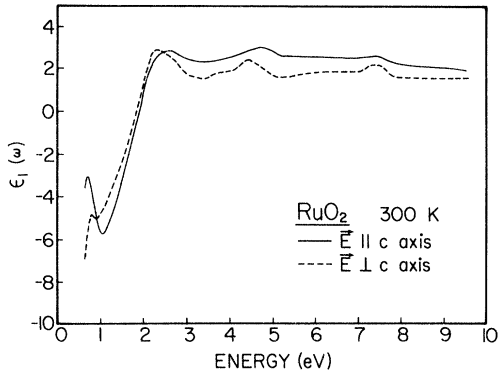

FIG. 3. Real part of the dielectric constant ϵ_1 of single-crystal rutile RuO_2 for $\vec{E}||c$ and $\vec{E}\perp c$.

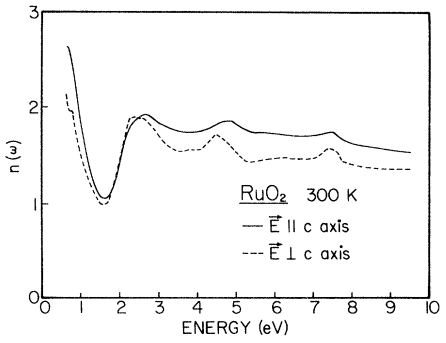

FIG. 5. Real part of refractive index n of single-crystal rutile RuO_2 for $\vec{E}||c$ and $\vec{E}\perp c$.

IrO_2. We have denoted the structural features in ϵ_2 related to those in the reflectivity spectra.

IV. DISCUSSION OF RESULTS

In the rutile structure each metal atom is surrounded by a nearly octahedral array of six oxygen atoms. The octahedral component of the ligand field causes metal d levels to be split into triply degenerate t_{2g} and doubly degenerate e_g components.[33] The t_{2g} and e_g degeneracies are lifted by the orthorhombic distortion. In these materials, the ten metal-atom d-states, which form the conduction bands, are separated by an energy gap from the 12 oxygen $2p$ states, which constitute the valence bands. The position of the Fermi level depends on the number of d electrons. In RuO_2 with four d electrons and in IrO_2 with five d electrons per metal atom the Fermi level will lie in the d-band complex.

In order to analyze our experimental results, we have made use of two recent theoretical works as well as past experimental studies of related materials such as TiO_2 and VO_2. Mattheiss has calculated the band structure as well as the density of states of the valence and conduction bands of RuO_2 and IrO_2.[34] Posternak *et al.* have calculated the joint density of states for rutile NbO_2, which has one d electron per metal atom.[35] They have also determined the band structure and individual density of states for this material.[35] Reflectivity and ϵ_2 spectra of rutile TiO_2 have been reported by Cardona and Harbeke who have studied in detail the optical properties and band structure of wurtzite-type crystals and rutile.[24] Finally, Verleur *et al.* have carried out a detailed optical investigation of VO_2, which undergoes a sharp semiconductor to metal(rutile) transition at 68 °C.[25]

A. RuO_2

Shown in Fig. 11 are the valence (oxygen p states) and conduction (Ru metal d states) band density of states for RuO_2 from Ref. 34. The effect of the crystal-field splittings of the d electron states

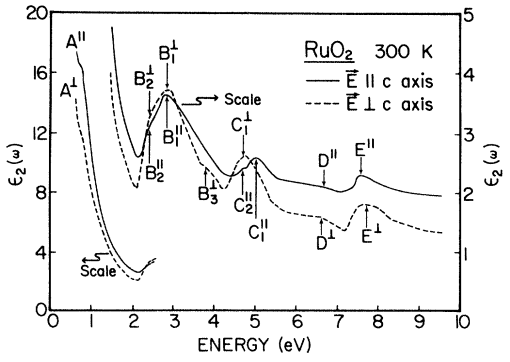

FIG. 4. Imaginary part of the dielectric constant, ϵ_2 of single-crystal rutile RuO_2 for $\vec{E}||c$ and $\vec{E}\perp c$.

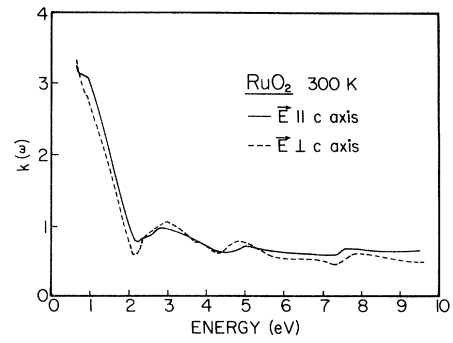

FIG. 6. Imaginary part of refractive index k of single-crystal rutile RuO_2 for $\vec{E}||c$ and $\vec{E}\perp c$.

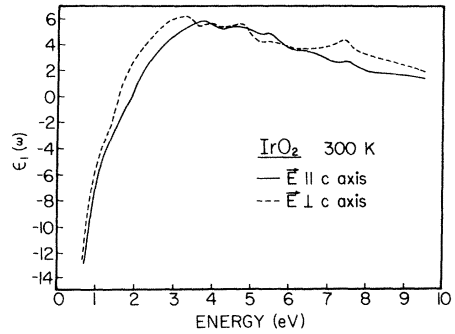

FIG. 7. Real part of the dielectric constant ϵ_1 of single-crystal rutile IrO_2 for $\vec{E}||c$ and $\vec{E}\perp c$.

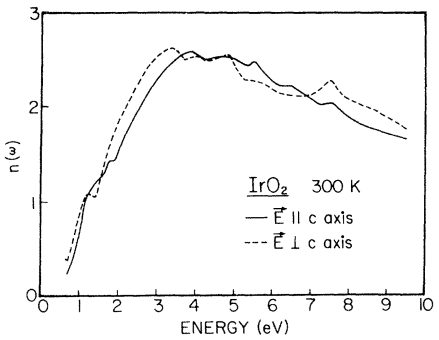

FIG. 9. Real part of refractive index n of single-crystal rutile IrO_2 for $\vec{E}||c$ and $\vec{E}\perp c$.

into t_{2g} and e_g bands is indicated. As shown by the position of the Fermi level, E_F, the t_{2g} orbitals are partially filled, while the e_g orbitals are empty. We note that the width of the t_{2g} bands is nearly 2.4 eV and the p-d band gap is approximately 2.3 eV. However, Mattheiss has pointed out his calculations tend to overestimate the p-d gap by several electron volts.

As shown in Fig. 4, the first major structure in $\epsilon_2(\omega)$ is the large peak A which is observed for both polarizations below ~ 2 eV. This pronounced feature is due primarily to free-carrier absorption with some contribution from d-electron intraband transitions (indicated by the small structure) within the t_{2g} manifold ($d_1 \rightarrow d_2$ in Fig. 11). Evidence for this assignment of A comes from several considerations including the optical properties of VO_2, which undergoes a sharp transition at 68 °C (T_c) from the semiconducting monoclinic phase to the metal rutile phase (with one d electron per metal atom). In this material the corresponding low-energy peak appears at temperatures above T_c and is absent below it[25,36] and hence is clearly related to the d electrons. Also such a low-energy feature is not observed in the optical constants of TiO_2,[24] which has the rutile structure with no d electrons. The joint-density-of-states calculation for NbO_2 shows a pronounced bump in the region below 2 eV (with a maxima around 1.5 eV) which is a result of d electron intraband transitions within the t_{2g} manifold.[35] Thus, these intraband transitions are probably responsible for the peak ($\vec{E}||c$) and shoulder ($\vec{E}\perp c$) on the large-A feature (see Fig. 4). The spectral dependence of the $\epsilon_1(\omega)$ curve (see Fig. 3) below about 3 eV is is similar to that for materials which have both free-electron and d-band contributions to the optical properties.[32]

The structure at photon energies above about 2.5 eV is due to $p \rightarrow d$ interband transitions. Similar features are seen for both phases of VO_2.[25,36] The first $p \rightarrow d$ peak in ϵ_2, represented by B_1, appears at approximately 2.8 eV. However, in the basis of Fig. 11 we expect it to be due to transitions from the valence states p_1 to conduction states d_2 and should occur at about 3.9 eV. This discrepancy be-

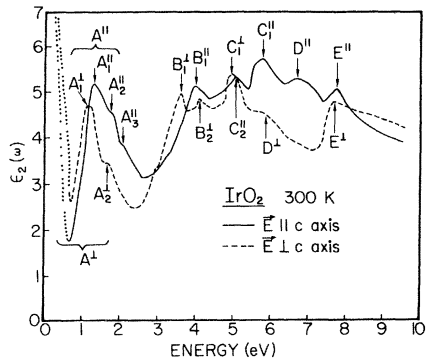

FIG. 8. Imaginary part of the dielectric constant ϵ_2 of single-crystal rutile IrO_2 for $\vec{E}||c$ and $\vec{E}\perp c$. Dotted lines correspond to extrapolated regions of Fig. 2.

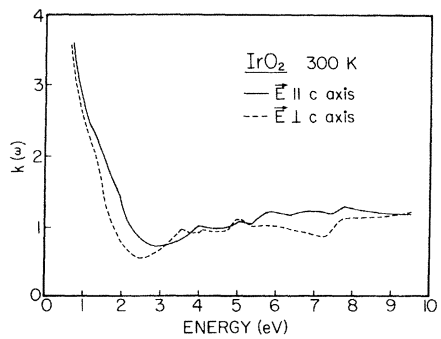

FIG. 10. Imaginary part of refractive index k of single-crystal rutile IrO_2 for $\vec{E}||c$ and $\vec{E}\perp c$.

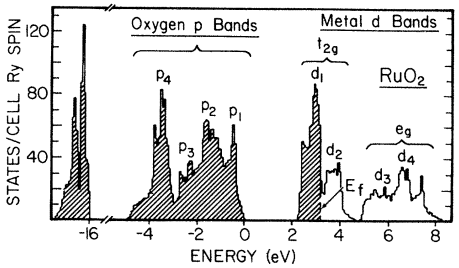

FIG. 11. Density of states for the valence (oxygen p levels) and conduction (metal d levels) bands of RuO_2 from Ref. 34. The ligand field splitting of the d levels into t_{2g} and e_g complexes is indicated.

tween the theoretically calculated density of states and our experimental results can be resolved if the p-d band gap is reduced by ~ 1 eV. After such a band-gap adjustment is made we can tentatively assign the peaks in ϵ_2 at about 5 eV (see Fig. 4) to transitions from p_3 states to d_2 states and the peaks at about 7.5 eV to transitions from p_2 to d_4 states.

B. IrO_2

The valence (oxygen p states) and conduction (Ir d states) band density of states for IrO_2 from Ref. 34 are shown in Fig. 12. The effect of the crystal field splittings of the d states into t_{2g} and e_g bands is also indicated. We see that in IrO_2, having five d electron per metal atom, the t_{2g} bands are more filled compared to those in RuO_2 which has four d electrons per metal atom. The d_2 manifold which is empty in the RuO_2 (see Fig. 11) is partially filled in IrO_2; the filled and empty parts have been indicated by d_2' and d_2'', respectively (see Fig. 12). However, the e_g bands are empty in IrO_2 as well

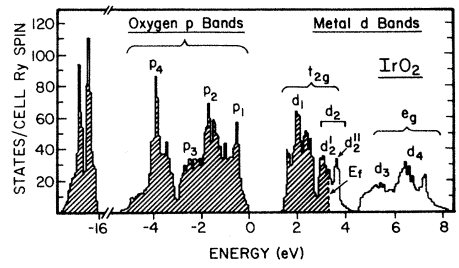

FIG. 12. Density of states for the valence (oxygen p levels) and conduction (metal d levels) bands of IrO_2 from Ref. 34. The ligand field splitting of the d levels into t_{2g} and e_g complexes is indicated.

Here, the width of the t_{2g} bands is nearly 2.8 eV and the p-d band gap as calculated by Mattheiss is approximately 1.5 eV.

Figure 8 shows the ϵ_2 spectra for $\vec{E}||c$ and $\vec{E}\perp c$ for IrO_2 in the energy range 0.5 to 9.5 eV. The dotted line corresponds to that in the reflectivity curves and is similar to ϵ_2 due to absorption by free charges only. The small features marked A_2 and A_3 are related to intraband electronic transitions within the t_{2g} complex, i.e., from filled d_1 and d_2' to empty d_2'' states shown in Fig. 12. The assignment of the A feature to free-carrier and intraband d-band effects is made since no $p \rightarrow d$ interband transitions are expected below 2 eV as indicated by the ϵ_1 curves[32] (see Fig. 7) and also by Fig. 12 which shows that the width of the filled t_{2g} band is ~ 2 eV. However, intraband transitions within the t_{2g} complex can occur up to ~ 2.8 eV.

Above ~ 3 eV, the structure in ϵ_2 is due to $p \rightarrow d$ interband transitions. We see from Fig. 8 that the first $p \rightarrow d$ peak in ϵ_2 appears at 4 eV for $\vec{E}||c$ but at ~ 3.5 eV for $\vec{E}\perp c$. On the basis of Fig. 12, however, we would expect it to occur at ~ 4 eV resulting from transitions from p_1 states to d_2' states. This difference between the theoretically expected and experimentally observed results can be resolved if we reduce the theoretically p-d band gap for IrO_2 by ~ 5 eV. Our reductions of the calculated band gaps for both RuO_2 and IrO_2 are consistent with the observation made by Mattheiss that his calculations tend to overestimate the band gap by several electron volts. After this band-gap adjustment is made, we can, as in the case of RuO_2, tentatively assign the features $C_2^{\parallel}$ and $C_1^{\perp}$ at about 5.2 eV and $C_1^{\parallel}$ at ~ 5.5 eV (see Fig. 8) to transitions from p_3 states to d_2'' states (see Fig. 12) and the stuctures denoted by $E^{\parallel}$ and $E^{\perp}$ at about 7.7 eV to transitions from p_2 to d_4 states. We note that the B_2 peak is narrower in IrO_2 than in RuO_2. This is probably because only the d_2'' part of the d_2 manifold is available as final states for transitions that give rise to this peak in IrO_2, whereas the whole d_2 manifold is available in RuO_2.

It is interesting to compare the ϵ_2 spectra of RuO_2 and IrO_2. Table I summarizes the energy positions of the major features in ϵ_2 of both RuO_2 and IrO_2 and our assignments of the interband transitions related to them. The comparison shows that both in RuO_2 and IrO_2, the ϵ_2 spectra above 2.5 and 3 eV, respectively, have three major features denoted by B, C, and E which can be accounted for by similar $p \rightarrow d$ transitions occurring in the two materials. For example, the B_1 features

TABLE I. Energy positions of the major structures in the ϵ_2 spectra of RuO_2 and IrO_2 (see Figs. 4 and 8) and our assignment of the interband transitions.

Structure denoted by	RuO_2[a]	IrO_2[b]
B_1	~2.8 eV ($p_1 \rightarrow d_2$)	~3.7 eV ($p_1 \rightarrow d_2''$)
C_1	~5.0 eV ($p_3 \rightarrow d_2$)	~5.5 eV ($p_3 \rightarrow d_2''$)
E	~7.5 eV ($p_2 \rightarrow d_4$)	~7.7 eV ($p_2 \rightarrow d_4$)

[a]After reduction of band gap by ~1 eV.
[b]After reduction of band gap by ~0.5 eV.

are associated with $p_1 \rightarrow d_2$ (or d_2'' in IrO_2) transitions, the features denoted by C_1 represent $p_3 \rightarrow d_2$ (or d_2'') transitions and the structures indicated by E have been assigned the $p_2 \rightarrow d_4$ transitions.

For a free-electron gas and in the absence of any interband transitions, the real part of the dielectric constant $[\epsilon_1 = 1 - (\omega_p^2/\omega^2)]$ becomes zero at the plasma frequency given by $\omega_p = (4\pi Ne^2/m^*)^{1/2}$, where N is the density of free electrons, e is the electronic charge, and m^* is the effective mass of the electron inside the metal. However, in the presence of interband transitions, experimental ϵ_1 has free and bound contributions and, starting from negative values, becomes zero at a frequency $\omega_i < \omega_p$ where $\hbar\omega_i$ indicates the threshold energy for interband transitions.[32] The ϵ_1 spectra for RuO_2 and IrO_2 in the energy range 0.5—9.5 eV are shown in Figs. 3 and 7, respectively. We note that the values of $\hbar\omega_i$ in the two cases are nearly 1.8 and 2.0 eV, respectively. Effective masses of the electron in RuO_2 and IrO_2 are not available in literature at present. Therefore, the exact values of the plasma frequencies for them cannot be estimated. However, it can be said that these will be well above the respective $\hbar\omega_i$ values.

We can calculate n_{eff}, an effective number of electrons per atom contributing to the optical properties in the finite energy range 0 to ω_0 with the help of a sum rule expressed by Phillip and Ehrenreich[37]:

$$n_{\text{eff}}(\omega_0) = \frac{m}{2\pi^2 Ne^2} \int_0^{\omega_0} \omega \epsilon_2(\omega) d\omega \ , \qquad (3)$$

where ω is the angular frequency of the light, m is the free electron mass, e is the electronic charge, and N is the number of atoms per unit volume. To apply Eq. (3) to RuO_2 (or IrO_2), it is more appropriate to define N as the number of Ru (or Ir) atoms per unit volume, in which case n_{eff} becomes the effective number of electrons pre Ru (or Ir) atom contributing to the optical absorption up to a frequency ω_0.

Figure 13 shows n_{eff} determined from the optical data of RuO_2 for both $\vec{E}||c$ and $\vec{E}\perp c$ in the energy range 0.5 to 9.5 eV. Near a photon energy of 2.5 eV there is an abrupt increase in the slope of n_{eff} which indicates the onset of interband transitions between the oxygen p bands and the ruthenium d bands. This conforms to our assignment of the structure in ϵ_2 above 2.5 eV to interband $p \rightarrow d$ optical transitions and that below 2.5 eV to free-electron absorption and intraband $d \rightarrow d$ transitons. For IrO_2, n_{eff} for both polarizations is shown in Fig. 14. In this case we seen an abrupt increase in the slope of n_{eff} at about 3 eV which again confirms our identification of the features in ϵ_2 above

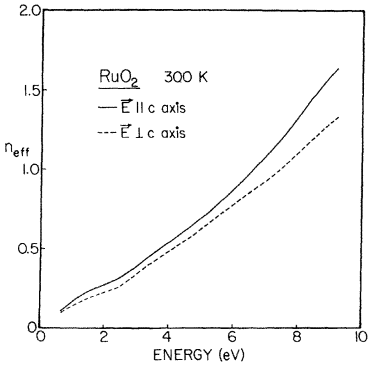

FIG. 13. Effective number of electrons per Ru atom, n_{eff}, contributing to the optical absorption in RuO_2 at room temperature for $\vec{E}||c$ and $\vec{E}\perp c$.

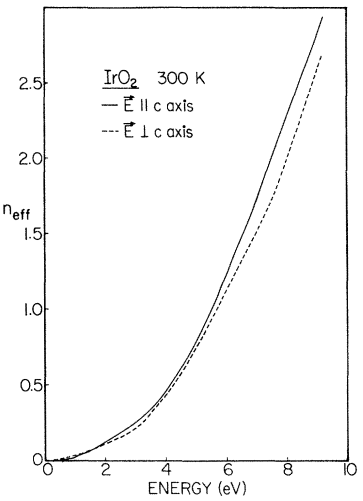

FIG. 14. Effective number of electrons per Ir atom, n_{eff}, contributing to the optical absorption in IrO_2 at room temperature for $\vec{E}||c$ and $\vec{E}\perp c$.

3 eV with interband transitions and those below 3 eV to intraband d transitions in addition to free-carrier absorption. The reason why the interband transtions in IrO_2 start at a higher energy than in RuO_2 is due mainly to the fact that the Fermi level E_F is higher in the former material.

More understanding of the nature of optical processes in RuO_2 and IrO_2 can be gained by comparison of our ϵ_2 spectra for those two materials with that of TiO_2 as obtained by Cardona and Harbeke.[24] It will be noticed that the structures in RuO_2 and IrO_2 are not nearly as sharp or as strong as in TiO_2 at ~ 4 eV. This is a very striking effect and could be explained in several possible ways. Lifetime broadening is perhaps the least likely explanation because of the very large broadening required. A more satisfactory explanation of the difference in the magnitude of the absorption is that, in TiO_2, the final states associated with the absorption peaks lie in the lowest conduction band whereas in RuO_2 and IrO_2, the lowest conduction bands are partially occupied by extra d electrons. Cardona and Harbeke[24] have suggested that in TiO_2, some of the optical structure up to 10 eV may arise from exciton effects. These effects are expected to give rise to sharp structure near critical points as observed near 4 eV. Such exciton effects would, however, be suppressed in RuO_2 and IrO_2 due to the screening by the large number of free carriers in these materials.

V. CONCLUSIONS

We have performed the first comprehensive optical investigation of the single-crystal rutile RuO_2 and IrO_2. The near-normal incidence reflectivity has been measured for $\vec{E}||c$ and $\vec{E}\perp c$ in the energy range 0.5—9.5 eV and we have deduced the optical constants from Kramers-Kronig analyses combinded with angular reflectivity measurements. The imaginary part of the dielectric constant (ϵ_2) has been compared with the band-structure and density-of-states calculations of Mattheiss as well as the theoretical work of Posternak *et al.*

For RuO_2, the structure in ϵ_2 below 2 eV is assigned to free-carrier absorption and $d \rightarrow d$ electron transitions. Above about 2.5 eV, all the features in ϵ_2 represent $p \rightarrow d$ interband transitions. Our results indicate that the calculation of Mattheiss has overestimated the p-d band gap in RuO_2 by ~ 1 eV.

For IrO_2, the structure in ϵ_2 below 2.5 eV is assigned to free-carrier absorption and $d \rightarrow d$ intraband transitions. Above about 3 eV, all the features in ϵ_2 represent $p \rightarrow d$ interband transitions. Our results indicate that the calculation of Mattheiss has overestimated the p-d band gap in IrO_2 by ~ 0.5 eV.

ACKNOWLEDGMENTS

We wish to acknowledge the extremely valuable contribution of Dr. L. I. Berger in helping to prepare the RuO_2 single crystals and Dr. F. M. Reames for supplying us the IrO_2 single crystals. This work has been supported by the U.S. Department of Energy under Contracts Nos. DE-AS02-80ET-2510 and DE-AC02-80ER-10654.

*Present address: Department of Energy and Environment, Building 801, Brookhaven National Laboratory, Upton, New York 11973.

[1]A. T. Kuhn and C. J. Mortimer, J. Electrochem. Soc. 120, 231 (1973).
[2]S. Puschaver, Chem. Ind. 236, 52 (1975).
[3]S. Trasatti and G. Buzzance, J. Electroanal. Chem. Interfacial Electrochem. 29, 635 (1971).

[4]W. O'Grady, C. Twakura, J. Huang, and E. Yeager, in *Electrocatalysis,* edited by M. W. Breiter (The Electrochemical Society Softbound Symposium Series, Princeton, N.J., 1974), pp. 268–297.

[5]L. D. Burke, O. J. Murphy, J. F. O'Neill, and S. Venkatesan, J. Chem. Soc., Faraday Trans. 1, 73, 1659 (1977).

[6]T. Kawai and T. Sakata, Chem. Phys. Lett. 72, 87 (1980).

[7]D. J. Pedder, Electrocomp. Sci. Tech. 2, 259 (1976).

[8]M. W. Shafer and J. Armstrong, IBM Tech. Discuss. Bull. 20, 4633 (1978).

[9]J. P. Hoare, *The Electrochemistry of Oxygen* (Interscience, New York, 1968).

[10]J. Horkans and M. W. Shafer, J. Electrochem. Soc. 124, 1202 (1977).

[11]See, for example, E. F. Chang, in *Nonemissive Electro-optic Display,* edited by A. R. Kmetz and F. K. von Willisen (Plenum, New York, 1976), p. 155.

[12]S. Gottesfeld, J. D. E. McIntyre, G. Beni, and J. L. Shay, Appl. Phys. Lett. 33, 208 (1978).

[13]G. Beni and J. L. Shay, Appl. Phys. Lett. 33, 567 (1978).

[14]D. A. J. Rand and R. Woods, J. Electroanal. Chem. Interfacial Electrochem. 55, 375 (1974).

[15]S. Gottesfeld and J. D. E. McIntyre, J. Eletrochem. Soc. 126, 742 (1979).

[16]S. Gottesfeld and S. Srinivasan, J. Electroanal. Chem. 86, 89 (1978).

[17]S. H. Glarum and J. H. Marshall, J. Electrochem. Soc. 127, 1467 (1980).

[18]W. C. Dautremont-Smith, G. Beni, L. M. Schiavone, and J. L. Shay, Appl. Phys. Lett. 35, 565 (1979).

[19]J. D. E. McIntyre, W. F. Peck, Jr., and S. Nakahara, J. Electrochem. Soc. 127, 1264 (1980).

[20]J. L. Shay, G. Beni, and L. M. Schiavone, Appl. Phys. Lett. 32, 942 (1978).

[21]W. D. Ryden, A. W. Lawson, and C. C. Sartain, Phys. Rev. B 1, 1494 (1970).

[22]G. K. Wertheim and H. J. Guggenheim, Phys. Rev. B 22, 4680 (1980).

[23]S. Trasatti and W. O'Grady, *Electrochemistry and Electrochemical Engineering,* edited by H. Gerischer and C. W. Tobias (Wiley, New York, 1981).

[24]M. Cardona and G. Harbeke, Phys. Rev. 137, 1467 (1965).

[25]H. W. Verleur, A. S. Barker, Jr., and C. N. Berglund, Phys. Rev. 172, 788 (1968).

[26]F. M. Reames, Mat. Res. Bull. 11, 1019 (1976).

[27]M. W. Shafer, R. A. Figat, B. Olsen, S. J. LaPlace, and J. Angilello, J. Electrochem. Soc. 126, 1625 (1979).

[28]Monsanto Corporation, distributed by Remet Corportation, Chadwick, N. Y. 13319.

[29]U. Gerhardt and G. W. Rubloff, Appl. Opt. 8, 305 (1969).

[30]S. S. M. Lu, F. H. Pollak, and P. M. Raccah, Phys. Rev. B 17, 1970 (1978).

[31]S. S. M. Lu, Ph. D. thesis, Yeshiva University, 1976 (unpublished).

[32]See, for example, F. Wooten, *Optical Properties of Solids* (Academic, New York, 1972), p. 62.

[33]See, for example, C. J. Ballhausen, *Introduction to Ligand Field Theory* (McGraw-Hill, New York, 1962).

[34]L. F. Mattheiss, Phys. Rev. B 13, 2433 (1976).

[35]M. Posternak, A. J. Freeman, and D. E. Ellis, Phys. Rev. B 19, 6555 (1979).

[36]V. G. Moderov and A. V. Rakov, Fiz. Tverd. Tela (Leningrad) 10, 1556 (1968). [Soviet Phys.—Solid State 10, 1231 (1968)].

[37]H. R. Philipp and H. Ehrenreich, Phys. Rev. 129, 1550 (1963).